Journal of Chemical Engineering of Japan, Vol. 36, No. 11, pp. 1397–1404, 2003 **Research Paper**

Preparation of Microporous Polypropylene Membrane via Thermally Induced Phase Separation as Support of Liquid Membranes Used for Metal Ion Recovery

SHENG SHENG FU[1], HIDETO MATSUYAMA[1],
MASAAKI TERAMOTO[1] AND DOUGLAS R. LLOYD[2]
[1]*Department of Chemistry and Material Technology, Kyoto Institute of Technology, Kyoto 606-8585, Japan*
[2]*Department of Chemical Engineering, University of Texas at Austin, Austin, Texas 78712, U.S.A.*

Keywords: Microporous Mmembrane, Thermally-Induced Phase Separation, Polypropylene, Supported Liquid Membrane, Uphill Transport

Microporous polypropylene (PP) membranes were prepared by the thermally induced phase separation (TIPS) technique and used as supports of liquid membranes. Several different quenching temperatures were used in the preparation of the microporous membranes. Membranes prepared by air-cooling and quenching in a water bath of 353 K showed higher porosity at the membrane surface compared with those made by quenching in a water bath of 303 K and in ice-water. A simplified one-dimensional heat transfer equation was solved to evaluate the temperature profile within the membrane to demonstrate the effect of quenching temperature on the final pore size distribution. The calculated result suggested that the asymmetric membrane structure formed by quenching in 303 K water and ice-water was not attributable to the temperature gradient.

Supported liquid membranes (SLMs) were prepared by impregnating a carrier solution in the prepared porous polypropylene membranes, and uphill transport of Ce(III) was investigated using octyl(phenyl)-*N*,*N*-diisobutyl-carbamoyl-methylphosphine oxide (CMPO) as a carrier, tributyl phosphate (TBP) as a modifier, and dodecane as a solvent. The membranes prepared by air-cooling showed higher permeability of Ce(III) than the commercial membrane.

Introduction

During the last two decades, the preparation of porous membranes via thermally induced phase separation (TIPS) has received extensive attention because TIPS is a versatile and simple technique for producing porous polymer membranes (Castro, 1981; Caneba and Soong 1985a, 1985b; Tsai and Torkelson, 1990; Lloyd *et al*., 1988, 1990, 1991; Berghmans *et al*., 1996). Since TIPS membrane formation is a non-equilibrium process, the cooling rate significantly influences the resulting membrane structure. The phase diagram for the isotactic polypropylene (iPP)-diphenyl ether (DPE) system is illustrated in **Fig. 1** (Matsuyama *et al*., 2000a). When a homogeneous polymer solution is quenched to a temperature below the cloud point, the solution is phase-separated into a polymer-rich phase and a polymer-lean phase. When the initial polymer concentration is higher than the concentration at the critical point, droplets of the polymer-lean phase are formed in a matrix of the polymer-rich phase. Decreasing the temperature below the crystallization curve induces solidification of the polymer. Since the droplet can grow in the temperature region from the cloud point to the crystallization temperature, faster cooling brings about smaller droplets (smaller pores) due to shorter time for the droplet growth.

The microstructure of the membrane is strongly dependent upon the preparation conditions. Polypropylene (PP) has been studied extensively for membrane applications because of its chemical stability and mechanical sturdiness. Lloyd and co-workers (Kim and Lloyd, 1991; Lim *et al*., 1991; Kim *et al*., 1991; Alwattari and Lloyd, 1991) reported the effects of thermodynamic properties, diluent mobility, and cooling rate on the membrane structure. The kinetics of phase separation in the iPP/DPE system has been investigated by the light scattering method in our laboratory (Matsuyama *et al*., 2000a). In addition, we studied the effect of polypropylene molecular weight on the porous membrane formation (Matsuyama *et al*., 2002).

Supported liquid membranes (SLMs) have been proposed as a possible technology for separation and concentration of metal ions because the required amount of extractant is much smaller than that used in

Received on April 8, 2003. Correspondence concerning this article should be addressed to H. Matsuyama (E-mail address: matuyama@chem.kit.ac.jp).

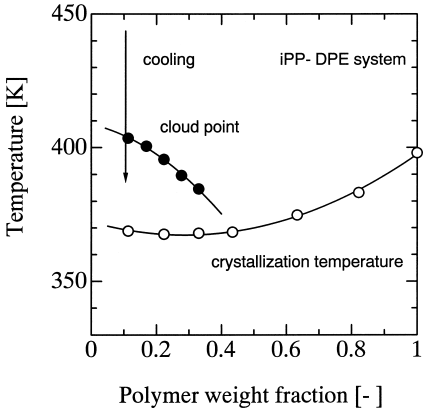

Fig. 1 Phase diagram for the iPP-DPE system. ●, cloud point; ○, dynamic crystallization temperature

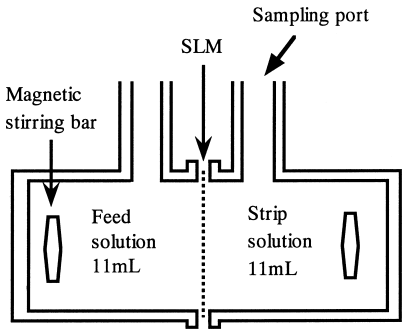

Fig. 2 Schematic diagram of the stirred permeation cell

solvent extraction and also the process is very simple (Noble and Way, 1987). In the SLM system, the microporous membrane is used as a support, which is impregnated with a carrier solution. In our previous work (Teramoto *et al.*, 2000a, 2000b), the transport mechanism of Ce through the SLM consisting of octyl(phenyl)-*N*,*N*-diisobutyl-carbamoyl methylphosphine oxide (CMPO) and tributyl phosphate (TBP) dissolved in dodecane was investigated as well as membrane stability. The chemical reaction describing the extraction of Ce(III) with CMPO from nitric acid solutions is expressed by (Danesi *et al.*, 1983):

$$Ce^{3+} + 3NO_3^- + \overline{3CMPO} \leftrightarrow \overline{Ce(NO_3)_3(CMPO)_3} \quad (1)$$

where the bars indicate species in the organic phase. In this membrane system, Ce(III) can be pumped from the feed to the strip side against its concentration gradient by keeping the NO_3^- concentration in the feed solution higher than that in the strip solution.

In the previous studies on the SLM, commercial microporous membranes were used as the supports (Teramoto *et al.*, 2000a, 2000b). As far as we know, no studies on the preparation of these support membranes for the SLM system have been reported. In this work, microporous polypropylene membranes were prepared by the TIPS process and were applied to SLM systems as the support membranes. The relationship between the support membrane structure and the performance of the SLM was investigated.

1. Experimental

1.1 Materials

Isotactic polypropylene (iPP, M_w = 250,000) was purchased from Aldrich Chemical Inc. The diluent was diphenyl ether (DPE) (Nacalai Tesque Ltd., Japan). CMPO was purchased from Hokko Chemical Industry Ltd., Japan, and used as received. TBP and dodecane were supplied by Wako Pure Chemicals Ltd., Japan. A commercial microporous polypropylene membrane (thickness = 150 μm; pore size = 0.2 μm; porosity = 0.75) was purchased from Akzo Noble Faser AG, Membrana.

1.2 Preparation of flat membranes

The iPP was dissolved in DPE at 473 K in a test-tube at a polymer concentration of 10 wt%, and the test tube was sealed under Ar atmosphere. After 48 hours, the test-tube was cooled to room temperature in a water bath to obtain a homogeneous polymer-diluent sample. The sample was sliced into desired pieces and placed between two square glass plates with a width of 10 cm and thickness of 1.5 mm, and the sample was then re-melted by placing the glass plate assembly in an oven at 453 K. By inserting a Teflon film with a square opening between the glass plates, the thickness of polymer solution was adjusted to about 100 μm. The glass plates containing homogeneous iPP solution at 453 K were then air-cooled or quenched in a horizontal position in a water bath at a desired temperature to solidify the sample. The sample was then immersed in a methanol bath at room temperature for 1 day to extract the diluent and the methanol was evaporated to produce the microporous membrane.

1.3 Membrane transport experiments

The transport of Ce(III) was measured at 298 K by using a stirred permeation cell. The permeation cell and the procedure for the permeation experiment were the same as those reported in our previous paper (Teramoto *et al.*, 2000a). The permeation cell is schematically shown in **Fig. 2**. SLMs were prepared by impregnating the microporous iPP membranes (supports) with the liquid membrane solution consisting of a dodecane solution of 0.382 M CMPO and 0.868 M TBP. Feed solutions were prepared by dissolving nitrate salts of Ce(III), Fe(III) and Cr(III) in aqueous 0.05 M HNO_3/2.95 M $NaNO_3$ solutions. The concentrations of Ce(III), Fe(III) and Cr(III) were 500, 400 and 300 ppm, respectively. Fe(III) and Cr(III) were added to the feed solution to check the stability of SLM. In all transport experiments described below, the con-

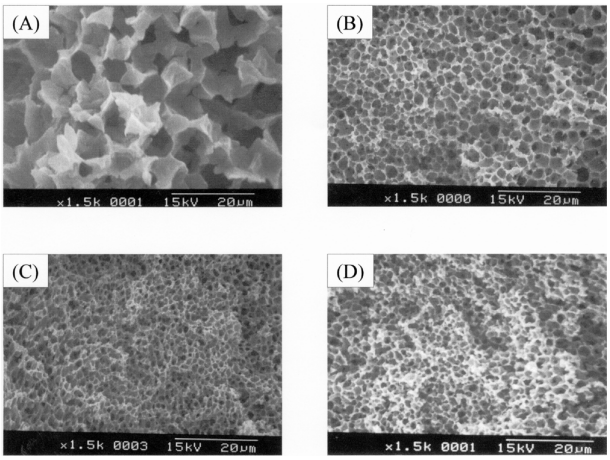

Fig. 3 SEM micrographs of the membrane cross-section: (A) air-cooling, (B) quenched in 353 K water, (C) quenched in 303 K water, (D) quenched in ice-water

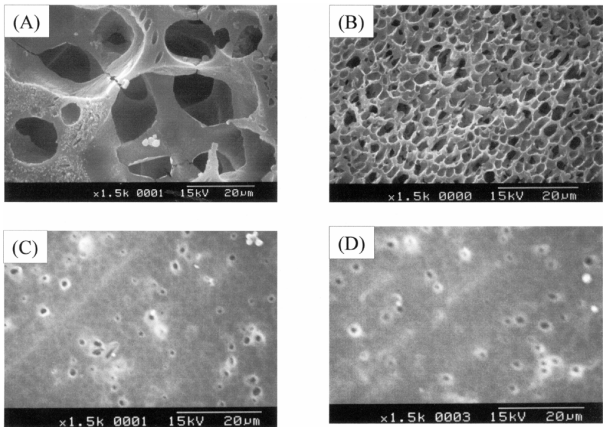

Fig. 4 SEM micrographs of membrane surfaces: (A) air-cooling, (B) quenched in 353 K water, (C) quenched in 303 K water, (D) quenched in ice-water

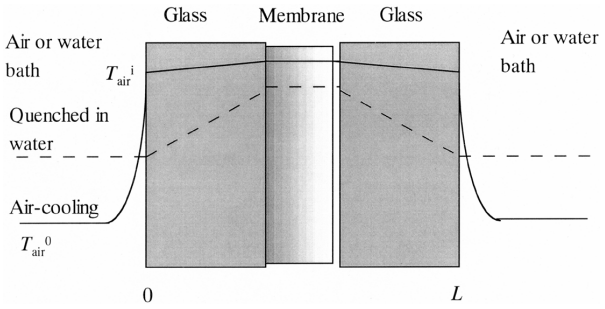

Fig. 5 Schematic illustration of the temperature profile during cooling of a polymer sample: — air-cooling; --- quenched in water

centrations of Fe(III) and Cr(III) in the strip solution were very low, which indicated that the SLM system was stable in the time scale of the transport experiment. The strip solutions were 0.3 M trisodium citrate (Na_3CA) aqueous solutions. This chelating agent was added to keep the free Ce(III) concentration in the strip solution very low. The volumes of the aqueous feed and strip solutions were kept constant at 11 mL in each experiment, and the membrane area was 4.15 cm^2. The stirring speeds of the feed and strip solutions were kept constant at 600 rpm in all experiments. Samples of 1 mL were withdrawn from the strip side of the cell to determine the metal ion concentration with an inductively coupled plasma spectroscope (ICPS-1000III, Shimadzu Co.), and 1 mL of the strip solution was added to the strip side to keep the volume of the solution constant.

2. Results and Discussion

2.1 Membrane morphology

The membranes were prepared by either air-cooling, quenching in a water bath at 353 or 303 K or quenching in ice-water. SEM micrographs of the cross-sections of each of these membranes are shown in **Fig. 3** as A, B, C and D. Each of the sample cross-sections has a high porosity. The porosity at membrane cross-section was 0.89, which was estimated from both polymer and diluent densities (Matsuyama *et al.*, 1999). The average pore size decreased according to the following order of cooling conditions: air-cooling, quenching in 353 K water and quenching in 303 K water or in ice-water. For example, the average pore sizes of membrane A and membrane D were 9.8 and 1.9 μm, respectively. These experimental results suggest that the pore size decreases with an increasing cooling rate. This is because faster cooling corresponds to shorter time for coarsening the droplets generated by liquid-liquid phase separation (Berghmans *et al.*, 1996).

The effect of the cooling condition on the surface structure of the membrane was also investigated. **Figure 4** shows the SEM micrographs of the surface structure of the membranes formed by the different cooling conditions. The membranes prepared by air-cooling and quenching in 353 K water have high surface porosity. On the other hand, the membranes prepared by quenching in 303 K water and in ice-water have lower porosity at the surface than in the cross-section. This means that these membranes had asymmetric structures.

A simplified one-dimensional heat transfer equation was sovled to calculate the temperature profiles in the quenched polymer samples in order to understand the effect of the quench condition on the membrane pore structure. **Figure 5** shows the schematic illustration of the temperature profile in the glass plates and the polymer samples. The heat transfer equation is derived with an energy balance:

$$\frac{\partial T}{\partial t} = \alpha_p \frac{\partial^2 T}{\partial x^2} \qquad \text{(Polymer solution)} \tag{2}$$

$$\frac{\partial T}{\partial t} = \alpha_g \frac{\partial^2 T}{\partial x^2} \qquad \text{(Glass plate)} \tag{3}$$

where T is temperature, t is the cooling time, x is the distance, and α_p and α_g are the thermal diffusivities of the polymer samples and the glass plate, respectively, and are assumed to be constant. The value of α_p is estimated by the following equation (Matsuyama *et al.*, 1999):

$$\alpha_p = \frac{\phi_1 k_1 + (1-\phi_1)k_2}{\left[\phi_1 C_{p1} + (1-\phi_1)C_{p2}\right]\left[\phi_1 \rho_1 + (1-\phi_1)\rho_2\right]} \tag{4}$$

where subscripts 1 and 2 refer to the polymer and the diluent, respectively, ϕ is the volume fraction, k is the thermal conductivity, C_p is the heat capacity. For calculations, the initial polymer sample is assumed to be at a uniform temperature T_0. In the case of air-cooling, the boundary layer between the glass plate and the air bulk phase is considered. The boundary conditions for air-cooling are expressed as follows (Matsuyama *et al.*, 1999):

$$t = 0; \quad T = T_0 \tag{5}$$

$$x = 0, L; \quad -k\frac{\partial T}{\partial x} = h\left(T_{air}^{i} - T_{air}^{0}\right) + \sigma\varepsilon_b\left(T_{air}^{i\,4} - T_{air}^{0\,4}\right) \tag{6}$$

$$h = 0.54\frac{k_g}{L_c}\left(G_r P_r\right)^{0.25} \tag{7}$$

$$G_r = L_c^3 \rho_g^2 g \beta \Delta T / \mu_g^2 \tag{8}$$

$$P_r = C_{pg}\mu_g / k_g \tag{9}$$

where h is the heat transfer coefficient, T^{i}_{air} and T^{0}_{air} are the temperatures of the air–glass interface and the air bulk phase, respectively; σ is a Stefan–Boltzmann constant; ε_b is the emissivity of the polymer solution; L_c is the characteristic length of the glass surface; k_g and C_{pg} are the thermal conductivity and heat capacity of the gas phase; ρ_g and μ_g are the total mass density of the gas phase and viscosity of the gas, respectively; G_r and P_r are the Grashof number for heat transfer and the Prandtl number; ΔT is the temperature difference between the air–glass interface and the gas bulk phase; the coefficient β is given by $(1/V)(\partial V/\partial T)_p$; g is the gravity constant. In the case of quenching in a water bath, the boundary layer between the glass plate and water was ignored. Thus, the temperature at the glass plate surface, which is contacted with water for the quench, is taken as the temperature of the water bath. Parameters used in these calculations are listed in **Tables 1** and **2**.

Table 1 Thermal conductivities, heat capacities and densities

	Thermal conductivity, k [W/(m K)]	Heat capacity, C_p [J/g K]	Density, ρ [g/cm^3]
DPE	0.13[a]	1.58[a]	0.96[a]
iPP	0.24[a]	5.80[a]	0.85[a]
Glass	0.76[b]	0.96[b]	2.70[b]
Air	3.5×10^{-2}[b]	1.02[a]	1.18×10^{-3}[c]

[a]Matsuyama *et al.* (1999); [b]Mizishina and Ogino (1981); [c]The Chemical Society of Japan (1993)

Table 2 Parameters used in calculation of heat transfer

μ_g* [Pas]	2.44×10^{-5}
β [K^{-1}]	3.36×10^{-3}
σ* [J/(m^{2}s K^4)]	5.67×10^{-8}
ε_b**	0.58
L_c [cm]	10.0

*Matsuyama *et al.* (1999)
**Mizishina and Ogino (1981)

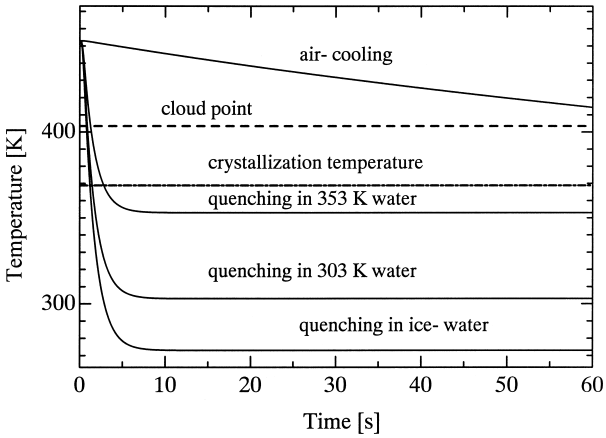

Fig. 6 Time-course of the calculated temperature at the sample center: - - - cloud point; —·—·— crystallization temperature

Figure 6 shows the time-course of the calculated temperature at the center of the polymer sample for several cooling conditions. The cloud point and the crystallization temperature are included in this figure. The cooling rate increases in the order of air-cooling,

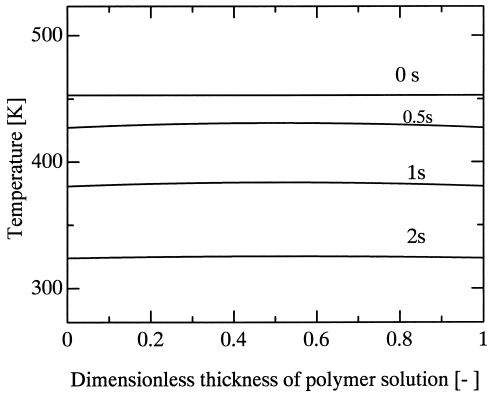

Fig. 7 Calculated sample temperature profiles at different times. Cooling condition: quenched in ice-water. The values of 0 and 1.0 of dimensionless thickness correspond to both interfaces contacted with glass plates

quenching in 353 K water, quenching in 303 K water, and quenching in ice-water. With increasing cooling rate, the time interval from the onset of phase separation (cloud point) to polymer solidification (crystallization temperature) decreases. This leads to smaller pores (Matsuyama *et al.*, 2000b). Thus, this calculation result indicates that the average pore size is expected to decrease in the above order. The experimental results shown in Fig. 3 agreed with this expectation.

The calculated temperature profiles in the polymer sample are shown in **Fig. 7**. The abscissa of this figure is the dimensionless thickness of polymer solution and the positions of 0 and 1 correspond to both interfaces contacted with glass plates. In the case of quenching in ice-water, which corresponds to the fastest cooling condition. The calculated temperature profile was almost flat and the surface temperatures were nearly equal to the temperature at the sample center. This somewhat surprising result is due to the much thicker glass plate than the polymer sample. The pronounced temperature gradient is formed in the glass plate rather than in the polymer solution.

As described above, an asymmetric pore structure was formed by quenching in ice-water. The asymmetric structure can usually be obtained by inducing a cooling rate gradient (Matsuyama *et al.*, 1999, 2000b). However, in this case, no cooling rate gradient was achieved, as shown in Fig. 7. Therefore, the interaction between the polymer and the glass plate was considered for the formation of the asymmetric structure.

When iPP-DPE solution is cooled from the homogeneous solution to a temperature below the cloud point, liquid-liquid phase separation occurs and droplets of polymer-lean phase are formed in a continuous matrix of the polymer-rich phase. The droplets grow with time through a process known as coarsening. The

Table 3 Surface tensions

	Surface tensions [dyn/cm]
iPP (423 K)	22.1*
DPE (423 K)	17.0**
Glass (296 K)	260**

*Brandrop and Immergut (1989); **The Chemical Society of Japan (1993)

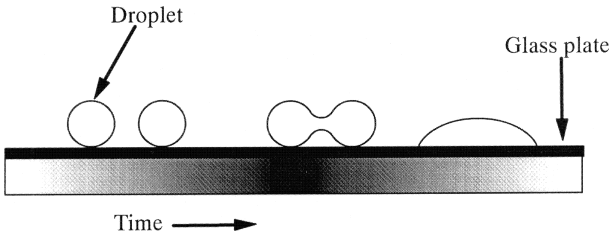

Fig. 8 Schematic coalescence process of two droplets on the glass plate

speculative coarsening process at the interface between the polymer solution and the glass plate is schematically shown in **Fig. 8**. In the early stage of phase separation, small droplets adhere to the glass plate at the small point. This is because the polymer-rich phase is more likely to contact with the glass plate than the polymer-lean phase because the surface tension of iPP is closer to that of the glass plate than DPE, as shown in **Table 3**. Since the polymer-lean phase becomes pore, the membrane at this point has much low porosity at the surface. When two droplets coalesce, a neck forms at junction, creating gradients in curvature that cause new droplets to be formed (Martula *et al.*, 2000). Then, a hemispheric droplet forms on the glass plate due to the swelling of the neck and a large amount of polymer-lean phase contacts with the glass plate. This leads to a higher porosity at the surface. When the cooling rate is too fast (quenching in ice-water and 303 K water), there is little time for the droplet growth until the polymer solution is solidified by the crystallization. In this situation, the small droplets adhere to the glass plate, and thus, the asymmetric structure with the low porosity at the surface is formed. On the other hand, when the cooling rate is slow (quenching in 353 K water and air-cooling), droplets can efficiently grow with time and the hemispheric droplets form on the glass surface. Therefore, a membrane with the high porosity at the surface is formed. Further study is necessary to confirm this speculated mechanism.

2.2 Permeation tests

Facilitated transport of Ce from an aqueous nitrate solution to an aqueous sodium citrate solution through a supported liquid membrane was performed. The porous membranes prepared by TIPS were used

as the supports for the liquid membrane. The flux J is obtained through the following equation:

$$J = -\frac{d[\mathrm{Ce}]_\mathrm{F}}{dt}\frac{V}{A} \tag{10}$$

where $[\mathrm{Ce}]_\mathrm{F}$ is the Ce(III) concentration in the feed solution, V is the volume of the feed solution and A is the membrane area. When the metal concentration in the feed solution is sufficiently high, the carrier is completely converted into the metal-carrier complex at the feed–membrane interface. Furthermore, when Na_3CA is added to the strip solution, the complex is completely decomposed at the strip-membrane interface. In this case, the flux is expressed as:

$$J = \frac{D_\mathrm{AM}}{L}[\mathrm{complex}]_\mathrm{Fi} \tag{11}$$

$$D_\mathrm{AM} = D_\mathrm{M}\frac{\varepsilon}{\tau} \tag{12}$$

where D_AM is the effective diffusion coefficient of the complex in membrane, D_M is the diffusion coefficient, ε is the surface porosity, and τ is the pore tortuosity. The complex concentration at the feed side interface $[\mathrm{complex}]_\mathrm{Fi}$ can be determined by solving the mass balance equation for the carrier, and knowing the relationship between the diffusion of the carrier and the diffusion of the complex. If we assume that the extraction of Ce(III) with CMPO is predominated by the 1:3 complex formation:

$$[\mathrm{carrier}]_0 = \frac{1}{2}\left([\mathrm{carrier}]_\mathrm{Fi} + [\mathrm{carrier}]_\mathrm{Si}\right) + \frac{3}{2}\left([\mathrm{complex}]_\mathrm{Fi} + [\mathrm{complex}]_\mathrm{Si}\right) \tag{13}$$

$$\frac{D_\mathrm{MB}}{L}\left([\mathrm{carrier}]_\mathrm{Si} - [\mathrm{carrier}]_\mathrm{Fi}\right) = 3\frac{D_\mathrm{AM}}{L}\left([\mathrm{complex}]_\mathrm{Fi} - [\mathrm{complex}]_\mathrm{Si}\right) \tag{14}$$

where subscript Fi denotes the feed-membrane interface, Si denotes the strip-membrane interface, 0 is an initial concentration, D_MB is the diffusion coefficient of carrier, L is the membrane thickness. Here, we assume $[\mathrm{carrier}]_\mathrm{Fi}$ and $[\mathrm{complex}]_\mathrm{Si}$ are equal to 0. If the molar volume ratio of CMPO to the complex is 1:3, the equation following relation between k_MB and k_MC holds according to the Wilke–Chang equation:

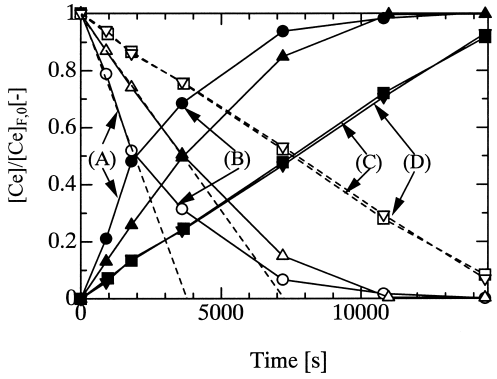

Fig. 9 Effect of support membrane on the permeation rate of Ce: (A) ○ (feed), ● (strip), membrane prepared by air-cooling (thickness = 120 μm); (B) △ (feed), ▲ (strip), membrane prepared by quenching in 353 K water (thickness = 120 μm); (C) □ (feed), ■ (strip), membrane prepared by quenching in 303 K water (thickness = 90 μm); (D) ▽ (feed), ▼ (strip), membrane prepared by quenching in ice water (thickness = 90 μm)

$$\frac{D_\mathrm{MB}}{D_\mathrm{AM}} = 3^{0.6} \tag{15}$$

By combining Eq. (13) with Eqs. (14) and (15), substitution of those into Eq. (11) gives

$$J = \frac{D_\mathrm{AM}}{L}\left(\frac{2}{3}\right)\left(\frac{3^{0.6}}{1+3^{0.6}}\right)[\mathrm{carrier}]_0 \tag{16}$$

Substitution of Eq. (16) into Eq. (10) and subsequent integration leads to the following equation:

$$\frac{[\mathrm{Ce}]_\mathrm{F}}{[\mathrm{Ce}]_\mathrm{F0}} = 1 - \left(\frac{D_\mathrm{AM}}{L}\right)\left(\frac{A}{V}\right)\left(\frac{2}{3}\right)\left(\frac{3^{0.6}}{1+3^{0.6}}\right)\left(\frac{[\mathrm{carrier}]_0}{[\mathrm{Ce}]_\mathrm{F0}}\right)t \tag{17}$$

where $[\mathrm{Ce}]_\mathrm{F0}$ is an initial Ce(III) concentration in the feed solution. The value of D_AM can be evaluated from the slopes of the straight lines in plots of $[\mathrm{Ce}]_\mathrm{F}/[\mathrm{Ce}]_\mathrm{F0}$ against time.

Figure 9 shows the effect of the support membranes on the permeation rate of Ce. The ordinate is the Ce(III) concentrations in the feed solution and in the strip solution divided by the initial Ce(III) concentration in the feed phase. The concentrations in the feed solution decreased with time, while those in the strip solution increased. After the concentration in the feed solution became equal to that in the strip solution, uphill transport of Ce(III) was achieved. The membrane prepared by air-cooling shows the highest permeation

Table 4 Effective diffusion coefficient of the complex in SLM

Cooling conditions	Air-cooling	Quenched in 353 K water	Quenched in 303 K water	Quenched in ice-water
D_{AM} [cm^2/s]	2.14×10^{-7}	1.04×10^{-7}	0.37×10^{-7}	0.36×10^{-7}

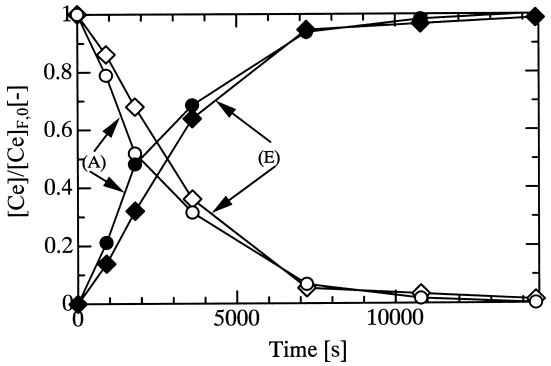

Fig. 10 Comparison of the membrane performance: (A) ○ (feed), ●(strip), membrane prepared by air-cooling (thickness = 120 μm); (E) ◇ (feed), ◆ (strip), commercial membrane (thickness = 150 μm)

rate of Ce(III), while those prepared by quenching in 303 K water (membrane C) and in ice-water (membrane D) showed the lowest permeabilities. As shown in Fig. 4, the surface porosities of the two membranes are very low. Therefore, the effective diffusion coefficient is deduced to be small from Eq. (12). In general, the flux is initially constant and then gradually decreases when $[Ce]_F$ becomes sufficiently lower compared with the carrier concentration. According to Eq. (17), when the flux is constant, a plot of $[Ce]_F/[Ce]_{F0}$ vs. time should yield straight lines. In Fig. 9, such straight lines are extended in broken lines, which allow one to evaluate D_{AM}. For the membranes A and B with high permeability, straight lines were obtained in the region of $[Ce]_F/[Ce]_{F0} > 0.5$; for membranes C and D with low permeability, straight lines were obtained in the region of $[Ce]_F/[Ce]_{F0} > 0.1$ as shown in Fig. 9. The calculated effective diffusivities are summarized in **Table 4**. The values of D_{AM} decrease with the cooling rate. Thus, the cooling rate has a significant effect on the surface porosity of the membrane, which affects the permeation rate of Ce.

Comparison of the permeation rate through the membrane prepared in this work with that through a commercial polypropylene membrane (thickness = 150 μm, pore size = 0.2 μm, porosity = 0.75) is shown in **Fig. 10**. The permeation rate of Ce(III) through the membrane prepared by air-cooling is faster than that through the commercial membrane. This means that our support membrane is superior to the commercial membrane for obtaining a higher flux.

Conclusion

Porous polypropylene (PP) membranes were prepared by the TIPS technique under various quench conditions. The membrane prepared by air-cooling has the largest average pore size. The pore size decreased with the increase of the cooling rate in the TIPS process. A simplified one-dimensional heat transfer equation was solved to evaluate the temperature profile across the membrane thickness to understand the effects of quenching temperature on the membrane pore size. The calculated result suggested that the asymmetric membrane structure formed by quenching a sample in 303 K water or ice-water was not attributable to the temperature gradient. In the permeation tests, the prepared membranes were used as supports of liquid membranes. The permeation rates were greatly influenced by the porous structures of the support membrane. The membrane prepared by the air-cooling showed a higher permeation rate than the commercial membrane.

Nomenclature

A	=	membrane area	[cm^2]
C_{p1}	=	heat capacity of polymer	[J/(g K)]
C_{p2}	=	heat capacity of diluent	[J/(g K)]
C_{pg}	=	heat capacity of the gas phase	[J/(g K)]
[Ce]	=	concentration of Ce	[mol/m^3]
[carrier]	=	concentration of the carrier	[mol/m^3]
[complex]	=	concentration of the Ce-CMPO complex	[mol/m^3]
D_{AM}	=	effective diffusion coefficient of the complex in membrane	[cm^2/s]
D_M	=	diffusion coefficient of the complex in membrane	[cm^2/s]
D_{MB}	=	diffusion coefficient of the carrier	[cm^2/s]
G_r	=	Grashof number	[—]
g	=	gravity constant	[m/s^2]
h	=	heat transfer coefficient	[W/(m^2 K)]
J	=	flux	[mol/(m^2 s)]
k_1	=	thermal conductivity of polymer	[W/(m K)]
k_2	=	thermal conductivity of diluent	[W/(m K)]
k_g	=	thermal conductivity of the gas phase	[W/(m K)]
L	=	membrane thickness	[cm]
L_c	=	characteristic length of the glass surface	[cm]
P_r	=	Prandtl number	[—]
T	=	temperature	[K]
T^i_{air}	=	temperature of the air–glass interface	[K]
T^0_{air}	=	temperature of the air bulk phase	[K]
t	=	time	[s]
V	=	volume of feed solution	[cm^3]
x	=	distance	[m]
α_g	=	thermal diffusivity of the glass plate	[cm^2/s]
α_p	=	thermal diffusivity of polymer solution	[cm^2/s]
β	=	$(1/V)(\partial V/\partial T)_P$	[1/K]

ΔT	=	temperature difference between the air–glass plate and the gas bulk phase	[K]
ε	=	surface porosity	[—]
ε_b	=	emissivity of polymer solution	[—]
μ_g	=	viscosity of the gas phase	[Pa s]
ρ_g	=	total mass density of the gas phase	[g/cm^3]
σ	=	Stefan–Boltzmann constant	[J/(m^{2}s K^4)]
τ	=	tortuosity	[—]
ϕ	=	volume fraction	[—]

<Subscript>

F	=	feed solution
Fi	=	feed-membrane interface
F0	=	initial value in feed solution
Si	=	strip-membrane interface
0	=	initial value
1	=	polymer
2	=	diluent

<Superscript>

–	=	species in organic phase

Literature Cited

Alwattari, A. A. and D. R. Lloyd; "Microporous Membrane Formation via Thermally Induced Phase Separation. VI. Effect of Diluent Morphology and Relative Crystallization Kinetics on Polypropylene Membrane Structure," *J. Membrane Sci.*, **64**, 55–68 (1991)

Berghmans, S., H. Berghmans and H. E. H. Meijer; "Spinning of Hollow Porous Fibres via the TIPS Mechanism," *J. Membrane Sci.*, **116**, 171–189 (1996)

Brandrop, J. and E. H. Immergut; Polymer Parameters Handbook, 3rd ed., p. VI/525, Wiley, New York, USA (1989)

Caneba, G. T. and D. S. Soong; "Polymer Membrane Formation through the Thermal-Inversion Process. 1. Experimental Study of Membrane Structure Formation," *Macromolecules*, **18**, 2538–2545 (1985a)

Caneba, G. T. and D. S. Soong; "Polymer Membrane Formation through the Thermal-Inversion Process. 2. Mathematical Modeling of the Membrane Structure Formation," *Macromolecules*, **18**, 2545–2555 (1985b)

Castro, A. J.; "How to Design Liquid Membrane Separations," U.S. Patent 4,247,489 (1981)

Danesi, P. R., E. P. Horwitz and P. G. Rickert; "Rate and Mechanism of Facilitated Americium(III) Transport through a Supported Liquid Membrane Containing a Bifunctional Orgaophosphorus Mobile Carrier," *J. Phys. Chem.*, **87**, 4078–4715 (1983)

Kim, S. S. and D. R. Lloyd; "Microporous Membrane Formation via Thermally Induced Phase Separation. III. Effect of Thermodynamic Interactions on the Structure of Isotactic Polypropylene Membranes," *J. Membrane Sci.*, **64**, 13–29 (1991)

Kim, S. S., G. B. A. Lim, A. A. Alwattari, Y. F. Wang and D. R. Lloyd; "Microporous Membrane Formation via Thermally Induced Phase Separation. V. Effect of Diluent Mobility and Crystallization on the Structure of Isotactic Polypropylene Membrane," *J. Membrane Sci.*, **64**, 41–53 (1991)

Lim, G. B. A., S. S. Kim, Q. Ye, Y. F. Wang and D. R. Lloyd; "Microporous Membrane Formation via Thermally Induced Phase Separation. IV. Effect of Isotactic Polypropylene Crystallization Kinetics on Membrane Structure," *J. Membrane Sci.*, **64**, 31–40 (1991)

Lloyd, D. R., J. W. Barlow and K. E. Kinzer; "Microporous Membrane Formation via Thermally Induced Phase Separation," New Membrane Materials and Processes for Separation, K. K. Sirkar and D. R. Lloyd, eds., AIChE Symp. Ser., No. 261, American Institute of Chemical Engineers, New York, USA (1988)

Lloyd, D. R., K. E. Kinzer and H. S. Tseng; "Microporous Membrane Formation via Thermally Induced Phase Separation. I. Solid-Liquid Phase Separation," *J. Membrane Sci.*, **52**, 239–261 (1990)

Lloyd, D. R., S. S. Kim and K. E. Kinzer; "Microporous Membrane Formation via Thermally Induced Phase Separation. II. Liquid-Liquid Phase Separation," *J. Membrane Sci.*, **64**, 1–11 (1991)

Martula, S. D., T. Hasegawa, D. R. Lloyd and R. T. Bonnecaze; "Coalescence-Induced Coalescence of Inviscid Droplets in a Viscous Fluid," *J. Colloid and Interface Sci.*, **232**, 241–253 (2000)

Matsuyama, H., S. Berghmans and D. R. Lloyd; "Formation of Anisotropic Membranes via Thermally Induced Phase Separation," *Polymer*, **40**, 2289–2301 (1999)

Matsuyama, H., S. Kudari, H. Kiyofuji and Y. Kitamura; "Kinetic Studies of Thermally Induced Phase Separation in Polymer-Diluent System," *J. Appl. Polym. Sci.*, **76**, 1028–1036 (2000a)

Matsuyama, H., M. Yuasa, Y. Kitamura, M. Teramoto and D. R. Lloyd; "Structure Control of Anisotropic and Asymmetric Polypropylene Membrane Prepared by Thermally Induced Phase Separation," *J. Membrane Sci.*, **179**, 91–100 (2000b)

Matsuyama, H., T. Maki, M. Teramoto and K. Asano; "Effect of Polypropylene Molecular Weight on Porous Membrane Formation by Thermally Induced Phase Separation," *J. Membrane Sci.*, **204**, 323–328 (2002)

Mizishina, T. and F. Ogino; Transport Phenomena, p. 317, Sangyozusyo, Toyko, Japan (1981)

Noble, R. D. and J. D. Way; Liquid Membranes: Theory and Applications, ACS Symp. Ser., American Chemical Society, Washington, D.C., USA (1987)

Teramoto, M., S. S. Fu, K. Takatani, N. Ohnishi, T. Maki, T. Fukui and K. Arai; "Treatment of Simulated Low Level Radioactive Wastewater by Supported Liquid Membranes: Uphill Transport of Ce(III) using CMPO as Carrier," *Sep. Purif. Technol.*, **18**, 57–69 (2000a)

Teramoto, M., Y. Sakaida, S. S. Fu, N. Ohnishi, H. Matsuyama, T. Maki, T. Fukui and K. Arai; "An Attempt for the Stabilization of Supported Liquid Membrane," *Sep. Purif. Technol.*, **21**, 137–144 (2000b)

The Chemical Society of Japan, ed.; Handbook of Chemistry, 4th ed., p. II-78, Maruzen, Tokyo, Japan (1993)

Tsai, F.-J. and J. M. Torkelson; "Roles of Phase Separation Mechanism and Coarsening in the Formation of Poly(methylmethacrylate) Asymmetric Membranes," *Macromolecules*, **23**, 775–784 (1990)